Gapless States in Microwave Artificial Graphene

Yulia N. Dautova,[1, a)] Andrey V. Shytov,[1] Ian R. Hooper,[1] J. Roy Sambles,[1] and Alastair P. Hibbins[1]
Department of Physics and Astronomy, University of Exeter, Exeter, Devon EX4 4QL, United Kingdom.

(Dated: 8 May 2017)

A microwave analogue of graphene comprised of cylindrical metallic rods arranged in a honeycomb array is fabricated. Dispersion curves of the bound electromagnetic eigenmodes of the system were experimentally determined by measuring the electric near-fields just above the surface. Two linear crossings are evident in these dispersion curves at each K and K' points of the Brillouin zone, mimicking the well-celebrated Dirac cones in graphene.

Graphene, the forefather of the 2D materials family, remains the focus of interest of various research communities, owing to its unusual electronic band structure, which arises from its honeycomb lattice and results in a number of distinctive effects. These include phenomena such as Klein tunnelling, pseudo-magnetic fields, and the anomalous quantum Hall effect.[1,2] There have been several studies on artificial analogies of graphene for electronic, acoustic, and photonic waves in recent years,[3] all of which have demonstrated the presence of Dirac crossings in their band structure. These include: using an AFM tip to arrange carbon monoxide molecules into a honeycomb structure, where a Dirac crossing was observed in the electronic band structure[4]; in photonic crystals made of dielectric elements, where Dirac crossings were observed in the photonic band structure[5,6]; and in hexagonal arrays of rigid cylinders placed in water, and in holes drilled in polymer glass, where the Dirac crossings were observed in the band structure for acoustic waves[7,8]. Graphene-inspired arrays of metallic particles have also been considered theoretically, and were shown to possess collective plasmon modes, full analogues to the electronic states in graphene.[9,10]

No experimental observations of a Dirac dispersion in the electromagnetic guided modes supported by a honeycomb array of metallic elements have been reported. In this work, we find two Dirac crossings at each K and K' points of the hexagonal Brillouin zone, a feature that has not been observed in graphene or other artificial graphene systems. We attribute this to the presence of higher order modes associated with individual rods. We confirm our findings with numerical, full-wave finite-element simulations, which agree very well with our experiment.

Steel cylindrical rods of diameter $d = 2$ mm and length $l = 15$ mm were inserted into a rigid foam slab (relative permittivity of $\epsilon_r = 1.05$), and arranged in a honeycomb array with a period of $a = 5$ mm (see Figure 1). The area of the sample was [250×300 mm] and approximately 2400 rods were used. Electromagnetic modes within the sample were excited and detected using two stripped-end near-field antennas, connected to a microwave vector network analyser (VNA). Both antennas were placed with their coaxial axes normal to the sample surface with the metal tips approximately 0.5 mm away from the surface and on opposite sides of the sample (to limit direct radiation transfer between the antennas). The near field of the source antenna provides sufficient in plane momentum to excite bound (i.e. non-radiative) modes in the foam-rod slab. To characterise the electromagnetic modes, the detecting probe was raster scanned across the sample surface with 1 mm step spacing. The amplitude and relative phase of local electric field (predominantly the z-component, due to the orientation of the antenna) were measured at each spatial coordinate over a frequency range between 1 and 25 GHz, with 25 MHz steps. A Fast Fourier Transform (FFT) is then applied to the measured field-data at each frequency step, to produce a matrix of complex Fourier amplitudes. Peaks in these amplitudes correspond to strong coupling to modes of the system, and hence by plotting the Fourier magnitudes as function of frequency and/or momentum (k_x, k_y), the modes' dispersion and equi-energy contours can be observed. It is important to note that the absolute values

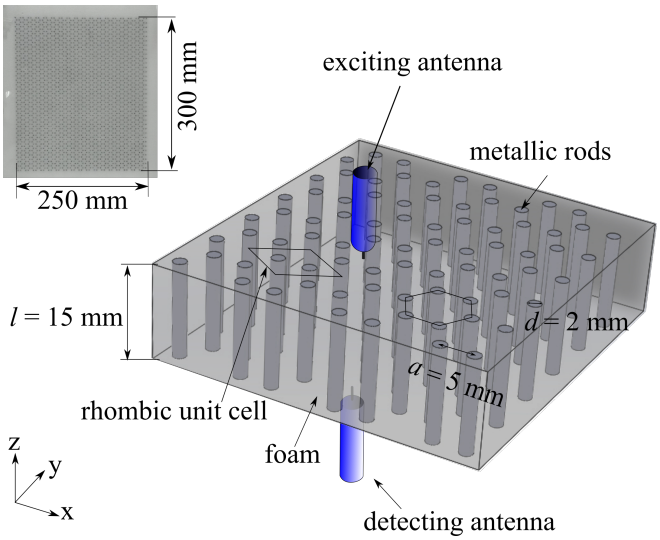

FIG. 1. Main panel: schematic representation of the sample. Metallic rods of $d = 2$ mm diameter and $l = 15$ mm length are arranged in a honeycomb array inside a supporting dielectric foam with lattice constant $a = 5$ mm. Inset: microwave graphene sample photograph.

[a)] Electronic mail: y.dautova@exeter.ac.uk

of the Fourier amplitudes are not important (since they depend on the geometry and method of excitation), but the position of the maxima gives a good estimation of the eigenfrequencies.

The COMSOL Multiphysics finite element method (FEM) frequency-domain solver was used to simulate the eigenmodes of the system. The metallic rods were treated as perfect electrical conductors embedded in material with relative permittivity of $\epsilon_r = 1.05$, with the remaining simulation domain described as air. "Perfectly matched layers" were placed as the top and bottom boundaries of the domain and Floquet periodic conditions were applied to the four remaining sides of the rhombic unit cell (see Figure 1) in order to simulate an infinite honeycomb array. An eigenfrequency solver was used to obtain the modes of the system, with different phase conditions applied between the Floquet boundaries in order to set the wave vector of the allowed modes, and the band structure of the system calculated..

The bound (non-radiative) modes of the sample are simply collective excitations of the rods, which disperse strongly on approach to each eigenfrequency of an isolated rod. Therefore, in the studied frequency range, two modes are observed, associated with the fundamental ($c/f = 2\lambda$) and 2nd harmonic ($c/f = \lambda$) rod resonances. On the Figure 2 Dirac crossings at the K point for each of these modes can be clearly seen for $f_{D1} = 8.325$ GHz and $f_{D2} = 16.325$ GHz.

The insets in Figure 2 show a zoomed-in view of the predicted dispersion curves in the vicinity of the two mode crossings and the norm of electric field distribution along rods in the unit cell. Using the linear approximation for the dispersion relation near the K point, we obtain the following values for the Dirac group velocities for the guided modes supported by our system: $v_{D1} = 1.9 \times 10^6$ ms^{-1} (0.006 of the light speed); $v_{D2} = 6 \times 10^6$ ms^{-1} (0.018 of the light speed). We also plot the equi-energy contours at the frequencies of the Dirac crossings in Figure 3. The six equivalent Dirac points are evident at both f_{D1} and f_{D2}.

Note that the upper modes that form the Dirac crossings are absent in the experimental data for the Γ-to-K direction within the 1st Brillouin zone (BZ). To observe this phenomena better we plot the dispersion in the extended zone scheme. For instance, the Γ-to-K direction becomes equivalent to the Γ-to-M direction when crossing the 1st BZ into the 3rd BZ. Similarly, the Γ-to-M direction becomes M-to-Γ equivalent in the 2nd BZ, and finally, going from the M-to-K direction brings us to the K-to-Γ equivalent in the 2nd BZ (see Figure 4(a)). Figure 4(b-c) show the extended zone. It is clear that the upper band of both modes are missing on the Γ-to-K plot in the 1st BZ (Figure 4(b)), however, they are present in the 2nd BZ in Figure 4(d).

The suppression of the upper bands in the 1st BZ along the $\Gamma - K$ direction can be shown to be a consequence of the symmetry of these modes. Let the electric field distribution of the mode with Bloch vec-

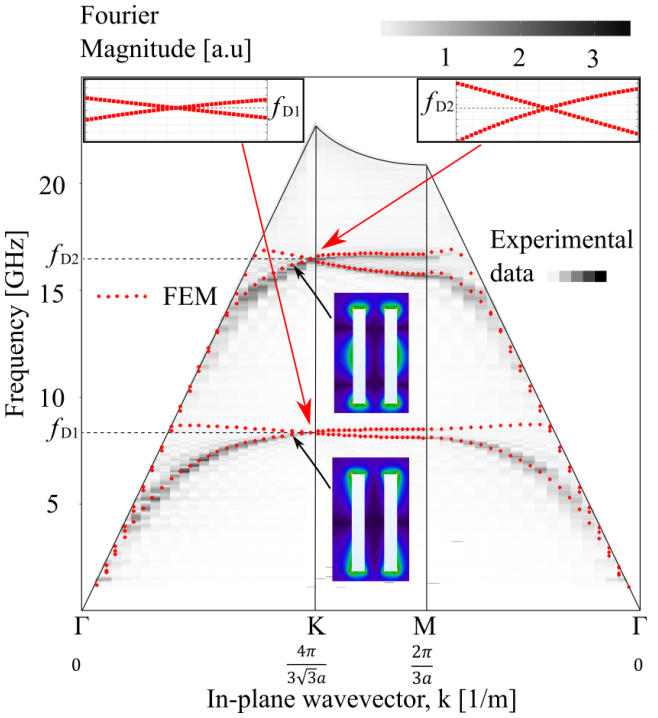

FIG. 2. FFTs performed on the experimental field maps just above the surface of the sample provide an indication of the dispersion of the bound electromagnetic modes. Solid black lines represent the light lines (maximum momentum available to a propagating photon). Red points are results of the FEM model. Insets: enlargements of the FEM predictions of the band structure in the vicinity of each Dirac crossing; FEM predictions of the norm of electric field for the 1st Dirac crossing at $f_{D1} = 8.325$ GHz (associated with the half wavelength resonance of the metallic rods) and for the 2nd Dirac crossing at $f_{D2} = 16.325$ GHz (associated with the full wavelength resonance of the metallic rods). The regions above the light lines correspond to radiative modes and are not under consideration. As such the experimental data in these regions has been removed.

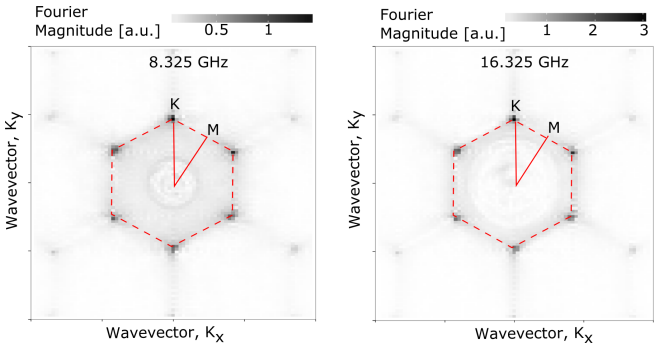

FIG. 3. Equi-energy contours at the frequencies of the Dirac crossings $f_{D1} = 8.325\ GHz$ (left) and $f_{D2} = 16.325\ GHz$ (right).

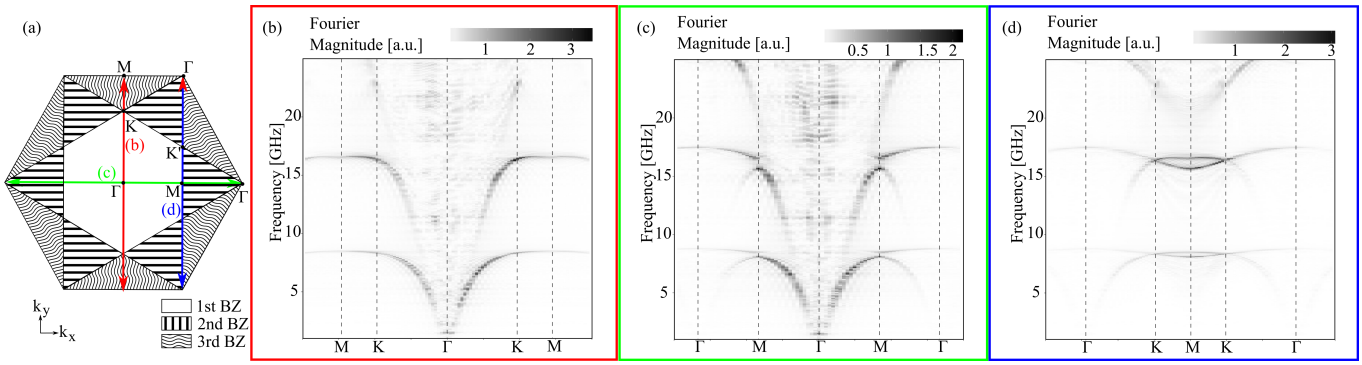

FIG. 4. (a) Structure of the honeycomb Brillouin zones. Colour arrows indicate the directions corresponding to the extended dispersion plots; (b-d) Experimentally determined dispersion relations along (b) Γ-to-K direction extended into the 3rd Brillouin zone to the M-equivalent point (along the red line in (a)), (c) Γ-to-M direction extended into the 2nd Brillouin zone to the Γ-equivalent point (along the green line in (a)), and (d) along the edge of the 1st Brillouin zone from M-to-K point and further into the 2nd Brillouin zone to the Γ-equivalent point (along the blue line in (a)).

tor $\mathbf{k}$ be $\mathbf{E}(\mathbf{r}) = \mathbf{E}_\mathbf{k}(\mathbf{r})e^{i\mathbf{kr}}$, so that the Bloch function $\mathbf{E}_\mathbf{k}(\mathbf{r})$ is periodic under translations by lattice vectors $\mathbf{T}$: $\mathbf{E}_\mathbf{k}(\mathbf{r}+\mathbf{T}) = \mathbf{E}_\mathbf{k}(\mathbf{r})$. (We treat $\mathbf{r}$ as a two-dimensional vector $\mathbf{r} = (x, y)$, assuming the observations are always performed in the same horizontal plane.) The Fourier transform of this field profile at the wave vector $\mathbf{q}$ can be recast in the form of an integral over a primitive cell as follows:

$$\int \mathbf{E}_\mathbf{k}(\mathbf{r})e^{-i\mathbf{qr}}\mathrm{d}\mathbf{r} = \sum_\mathbf{T}\int_S \mathbf{E}_\mathbf{k}(\mathbf{r})e^{i(\mathbf{k}-\mathbf{q})\mathbf{r}}e^{i\mathbf{T}(\mathbf{k}-\mathbf{q})}\mathrm{d}\mathbf{r} = 4\pi^2\sum_G \delta(\mathbf{q}-\mathbf{k}-\mathbf{G})\int_S \mathbf{E}_\mathbf{k}(\mathbf{r})e^{-i\mathbf{Gr}}\mathrm{d}\mathbf{r}, \quad (1)$$

where $\sum_\mathbf{T}$ is a sum over all translation vectors of the lattice, the integral on the right hand side is performed over a primitive cell, and $\mathbf{G}$ is an arbitrary reciprocal lattice vector, and $\delta(\mathbf{q}-\mathbf{k}-\mathbf{G})$ is the Dirac delta-function. Eq. (1) immediately follows from the standard identity from band theory:

$$\sum_\mathbf{T} e^{i\mathbf{T}(\mathbf{q}-\mathbf{k})\mathbf{r}} = 4\pi^2\sum_\mathbf{G}\delta(\mathbf{q}-\mathbf{k}-\mathbf{G}).$$

Eq. (1) shows that the Fourier transform vector $\mathbf{q}$ can differ from the Bloch vector by an arbitrary reciprocal lattice vector $\mathbf{G}$. In other words, every reciprocal lattice vector $\mathbf{G}$ contributes a replica of the mode at wave vector $\mathbf{q} = \mathbf{k} + \mathbf{G}$. The intensity of the replica depends on $\mathbf{G}$ via the integral on the right hand side of Eq. (1). Let us consider the case when the vector $\mathbf{q}$ is between Γ and K. This gives $\mathbf{G} = 0$ and $\mathbf{k} = \mathbf{q}$. Then, the integral over a unit cell vanishes if the Bloch mode is antisymmetric with respect to mirror reflection about the Γ-K line. This is indeed the case for the upper branch, as obtained by the FEM modeling, as can be seen in Figure 5. Therefore, the signal of this mode is indeed suppressed due to the vanishing integral in Eq. (1). For values of $\mathbf{q}$ outside of the 1st BZ, one has to employ a non-zero value of $\mathbf{G}$ in Eq.(1), so that the symmetry does not lead to suppression. This explains the re-emergence of the mode at larger values of $\mathbf{k}$ along the symmetry line.

Let us now explain how the absence of the modes arises from the honeycomb symmetry. Mirror reflections along the three Γ − K lines transform the lattice into itself, exchanging the A and B sub-lattices. In general, these mirror symmetries, are not a symmetry of individual Bloch modes: each mirror reflection transforms a mode at a wave vector $\mathbf{k}$ into a mode at its mirror

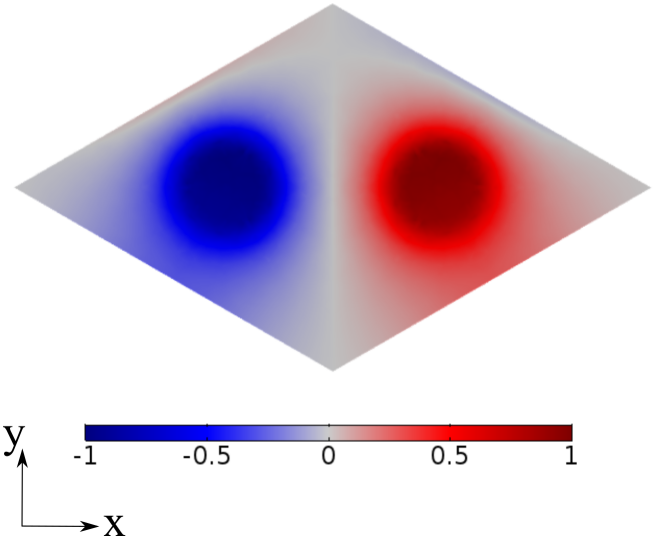

FIG. 5. Prediction of the normal component of electric field above the sample surface for $k_x = 0$ m^{-1} and $k_y = 300$ m^{-1} on the line from Γ-to-K for upper modes (normalised).

image $\mathbf{k}^\star$: $\mathbf{E}_\mathbf{k}(\mathbf{r}) \rightarrow \mathbf{E}_\mathbf{k}(\mathbf{r}^\star) \propto \mathbf{E}_{\mathbf{k}^\star}(\mathbf{r})$. The symmetry only implies that the two mirror modes have the same frequency, and one can construct odd/even functions by taking symmetric/antisymmetric combination of these. However, if the wave vector $\mathbf{k}$ lies on the $\Gamma - \mathrm{K}$ line it is unchanged under mirror reflection, $\mathbf{k} = \mathbf{k}^\star$, and the sublattice symmetry becomes the symmetry of each mode on this line. Hence, on the Γ-to-K line, each mode must be either symmetric or antisymmetric under the mirror reflection: $\mathbf{E}_\mathbf{k}(\mathbf{r}^\star) = \pm\mathbf{E}_\mathbf{k}(\mathbf{r})$. Using FEM modeling we find that the upper modes near the Dirac points are antisymmetric and, thus, their Fourier transform is zero in the 1st BZ as two sub-lattices give contributions of the opposite sign.

In conclusion, we have fabricated artificial "microwave graphene" made of metallic rods arranged in a honeycomb array and experimentally measured the confined eigenmodes it supports. We have determined the dispersion curves of this microwave graphene, and have shown two linear crossings at the K points of the hexagonal Brillouin zone, mimicking the well-celebrated Dirac cones in graphene. The presence of two Dirac points arises from two different modes supported by the individual rods.

Manipulation of the band structure may be used for engineering new materials which do not occur naturally but possess properties required for specific applications.[11,12] In the case of graphene, destroying the inversion symmetry between its two sublattices results in a bandgap opening at the Dirac point, while the Dirac point position itself and the slope of the crossings can be controlled by changing the structure parameters, i.e. honeycomb period and rod dimensions.[1,12,13] It is rather challenging to create a bandgap for true graphene but it is easily achievable in the artificial system such as that presented here where the lattice is created atom-by-atom. For electromagnetic waves, by combining gapless artificial graphene and the graphene with a purposely created bandgap it should be possible to construct 2D waveguides.[14]

The authors wish to acknowledge the financial support from the Engineering and Physical Sciences Research Council (EPSRC) of the United Kingdom, via the EPSRC Centre for Doctoral Training in Metamaterials (Grant No. EP/L015331/1). All data created during this research are openly available from the University of Exeters institutional repository at https://ore.exeter.ac.uk/.

[1] A. K. Geim and K. S. Novoselov, "The rise of graphene," Nature materials **6**, 183–191 (2007).
[2] A. C. Neto, F. Guinea, N. M. Peres, K. S. Novoselov, and A. K. Geim, "The electronic properties of graphene," Reviews of modern physics **81**, 109 (2009).
[3] M. Polini, F. Guinea, M. Lewenstein, H. C. Manoharan, and V. Pellegrini, "Artificial honeycomb lattices for electrons, atoms and photons," Nature nanotechnology **8**, 625–633 (2013).
[4] K. K. Gomes, W. Mar, W. Ko, F. Guinea, and H. C. Manoharan, "Designer dirac fermions and topological phases in molecular graphene," Nature **483**, 306–310 (2012).
[5] T. Ochiai and M. Onoda, "Photonic analog of graphene model and its extension: Dirac cone, symmetry, and edge states," Physical Review B **80**, 155103 (2009).
[6] M. Bellec, U. Kuhl, G. Montambaux, and F. Mortessagne, "Tight-binding couplings in microwave artificial graphene," Physical Review B **88**, 115437 (2013).
[7] X. Zhang and Z. Liu, "Extremal transmission and beating effect of acoustic waves in two-dimensional sonic crystals," Physical review letters **101**, 264303 (2008).
[8] D. Torrent and J. Sánchez-Dehesa, "Acoustic analogue of graphene: observation of dirac cones in acoustic surface waves," Physical review letters **108**, 174301 (2012).
[9] G. Weick, C. Woollacott, W. L. Barnes, O. Hess, and E. Mariani, "Dirac-like plasmons in honeycomb lattices of metallic nanoparticles," Physical review letters **110**, 106801 (2013).
[10] G. Weick and E. Mariani, "Tunable plasmon polaritons in arrays of interacting metallic nanoparticles," The European Physical Journal B **88**, 1–8 (2015).
[11] N. I. Zheludev and Y. S. Kivshar, "From metamaterials to metadevices," Nature materials **11**, 917–924 (2012).
[12] N. Meinzer, W. L. Barnes, and I. R. Hooper, "Plasmonic meta-atoms and metasurfaces," Nature Photonics **8**, 889–898 (2014).
[13] L. Tarruell, D. Greif, T. Uehlinger, G. Jotzu, and T. Esslinger, "Creating, moving and merging dirac points with a fermi gas in a tunable honeycomb lattice," Nature **483**, 302–305 (2012).
[14] A. Chutinan and S. Noda, "Waveguides and waveguide bends in two-dimensional photonic crystal slabs," Physical review B **62**, 4488 (2000).